# Colitis-induced visceral pain recruits central neurotensin neurons that modulate colonic sensitivity

**Authors**

Yu-Ting Cheng[1,2], Natalie MacKinnon-Booth[1], Yingfu Jiao[1], Jordan R. Robbins[1], Murillo Duarte-Silva[3], Perry E. Mitchell[3], Yuchu Liu[1], Omer Barkai[1,2], Keunjung Heo[1,2], Biyao Zhang[1], Bruna Lenfers Turnes[1,2], Meenakshi Rao[3] and Clifford J. Woolf[1,2]*

**Affiliations**

[1]F.M. Kirby Neurobiology Center, Boston Children's Hospital, Boston, MA, USA

[2]Department of Neurobiology, Harvard Medical School, Boston, MA, USA

[3]Division of Gastroenterology, Department of Pediatrics, Boston Children's Hospital and Harvard Medical School, Boston, USA

[*]Correspondence: clifford.woolf@childrens.harvard.edu

**Abstract**

Inflammatory bowel disease produces debilitating visceral pain that remains a major clinical challenge. Notably, many patients experience persistent pain even after the inflammation resolves, indicating a sustained sensitization of central neural circuits that drives enduring pain. The brainstem parabrachial nucleus integrates interoceptive signals from the gastrointestinal tract to elicit both pain perception and affective responses. Using activity-dependent mapping and an RNAscope assay, we identified a neurotensin (NT)-expressing neuronal population in the lateral PBN ($PBN_L$) that is selectively activated during dextran sulfate sodium-induced colitis. *In vivo* neural activity recordings demonstrate that $PBN_L$ NT neurons encode colon-derived nociceptive signals in an intensity-dependent manner. Silencing these neurons attenuates colonic reflexes evoked by luminal distension and normalizes aberrant gastrointestinal transit and nociceptive licking behavior in colitic mice. Pharmacological blockade of NT signaling alleviates colitis-associated hypersensitivity. These findings identify a central neural population that encodes visceral inflammation and regulates peripheral organ function, and pinpoints neurotensin as a promising therapeutic target to treat colitis-induced visceral pain.

## Introduction

Pain associated with inflammatory bowel disease (IBD) affects up to 10 million people worldwide and arises from the activation of nociceptor afferents by inflammatory responses mediated by a compromised epithelial lining of the gut barrier[1-3]. Clinical hallmarks of colitis include spontaneous abdominal pain, visceral hypersensitivity, and altered bowel function, such as diarrhea and dysmotility[4,5]. Current pharmacological treatments primarily target mucosal inflammation; however, tissue healing verified by endoscopy or histopathology, does not reliably produce symptomatic relief, with 30–50% of patients continuing to report persistent pain even after resolution of their inflammatory flare[6,7]. This suggests that a central neural sensitization may contribute to the maintenance of visceral pain independently of ongoing peripheral pathology[8-10].

The brainstem parabrachial complex serves as a key integrative hub that relays interoceptive and exteroceptive signals from the periphery to forebrain regions to elicit pain and affective perception[11-15]. Within this complex, the lateral parabrachial nucleus ($PBN_L$) primarily receives nociceptive input from the spinal dorsal horn via the anterolateral pathway and is engaged in acute and chronic pain states[16-18]. Genetic and circuit-level dissection of $PBN_L$ neuronal populations, together with an analysis of their neuropeptide signaling has begun to reveal a powerful leverage mechanism for modulating pain and its associated emotional disturbances[19-22]. However, despite accumulating evidence implicating the role of $PBN_L$ in somatosensory pain[23-26], the identity of those neuronal ensembles that encode visceral nociceptive signals, and if and how these influence organ function and visceral pain-related behavior, are unclear.

We identified a population of neurotensin (NT)-expressing neurons within the $PBN_L$ that is selectively activated during dextran sulfate sodium (DSS)-induced colitis and encodes colon-derived nociceptive information in an intensity-dependent manner. Silencing the $PBN_L$ NT neurons abrogated the exaggerated colonic reflexes evoked by pressure distension, while blockade of neurotensin signaling normalized the diarrhea and pain-associated behaviors induced by the colitis. These findings provide evidence for a central neural modulation of peripheral visceral function and pinpoint $PBN_L$ NT neurons as a mechanistically defined node linking visceral inflammatory pain and affective states, with promising implications for treating colitis-induced visceral pain.

102 **Results**

103 **Activation of nociceptors by colitis drives spontaneous nocifensive behaviors**

104 We modeled experimental colitis by administering 3% DSS into the drinking water of mice[27,28]
105 for 4 days and measured spontaneous pain-related behaviors together with abdominal allodynia
106 for 2 weeks to evaluate the temporal profile of altered nociceptive behavioral responses (**Fig.**
107 **1a**). Colon inflammation was confirmed by an infiltration of CD45-positive immune cells into
108 distal colon tissues 4 days after DSS exposure (D4) and 3 days after the DSS withdrawal (D7),
109 which progressively resolved over 2 weeks (**Fig. 1b,c**). Additionally, we monitored a reduction
110 of mouse body weight and water intake in DSS-treated WT mice compared to regular $H_2O$
111 drinking water controls, which gradually recovered on D14 (**Extended Data Fig. 1a,b**).
112
113 We implemented a supervised machine learning algorithm to automatically screen for pain-
114 related behavior signatures relevant to the DSS-induced colitis[29,30]. This analysis revealed a
115 significant increase in "lower body licking" encompassing abdominal and peri-anal licking
116 during the active inflammation, when compared with mice receiving regular $H_2O$ drinking
117 water (**Fig. 1d**). A licking bout was defined as contact between the snout and the abdominal or
118 peri-anal region sustained for at least two consecutive video frames. To interpret model features
119 underlying licking classification, we analyzed the 10 most informative features using SHAP
120 (Shapley additive explanations). Spatial features contributed most strongly to the model
121 performance, with the distance between the snout/neck and the tail base ranked as the top
122 feature, reflecting close proximity of the head to the lower body during licking behavior
123 (**Extended Data Fig. 2a**). Model performance improved with increasing training data, as
124 shown by the F1-score learning curve, and reached a plateau near 0.8 after approximately 6,000
125 labeled frames (**Extended Data Fig. 2b**). To further optimize classification performance, we
126 evaluated precision, recall, and F1-score across a range of discrimination thresholds on the
127 validation dataset. This analysis identified an optimal operating threshold centered around ~0.6,
128 which was used for subsequent behavioral quantification (**Extended Data Fig. 2c**).
129
130 A correlation between time spent licking and the stool-based disease activity index (DAI), a
131 score calculated as the sum of two components: stool consistency and fecal blood[28],
132 demonstrated a positive linear relationship in the DSS mice (**Fig. 1e**), suggesting that lower
133 body licking reflects the severity of colitis in mice. To measure colitis-induced mechanical
134 allodynia, which is analogous to the feature of abdominal tenderness on clinical examination,
135 we performed an up-down von Frey assay on the skin of the lower abdomen to calculate the

136 50% withdrawal threshold. We observed a profound decrease in the abdominal response
137 threshold during the DSS water treatment, which gradually recovered after DSS removal to
138 thresholds found in regular $H_2O$ regimen control mice (**Fig. 1f**). To examine the functional
139 relevance of the licking behavior during the 4-day DSS water regimen to pain, we used Nav1.8-
140 Cre mice that express either an inhibitory hM4Di receptor for chemogenetic inhibition, or
141 tdTomato as a control, in dorsal root ganglion nociceptor neurons that trigger nocifensive
142 reflexes in response to noxious stimuli (**Extended Data Fig. 3**). Mice where Nav1.8-lineage
143 nociceptors were temporarily silenced by activating hM4Di on receiving 0.1 mg/kg of
144 deschloroclozapine (DCZ)[31] once per day over the 4 days of DSS exposure, displayed a marked
145 reduction of nociceptive licking behavior and an attenuation of body weight loss (**Fig. 1g and**
146 **Extended Data Fig. 1a**). This analgesic-like effect persisted on D5 after the cessation of
147 Nav1.8 nociceptor silencing, but subsided by D7, when the behavior was indiscernible between
148 Nav1.8-tdTom and WT controls with DSS treatment. This reveals that the behavioral licking
149 signature tracks colitis severity and is triggered by Nav1.8-lineage nociceptors.
150
151 In parallel, we used an acute, mechanically induced visceral pain model by introducing graded
152 mechanical distension in the mouse distal colon (**Extended Data Fig. 4a,b**). To produce an
153 acute noxious colonic stimulus, a balloon was inserted and connected via a bifurcated tube to
154 an air-pressurized syringe and a manometer to enable controlled distension and pressure
155 monitoring. Acute colon distension at a pressure of 40 and 80 mmHg elicited pressure
156 intensity-dependent spontaneous behaviors, including abdominal licking, abdominal squashing
157 and hunching (**Extended Data Fig. 4c**), which were effectively diminished following Nav1.8-
158 nociceptor chemogenetic silencing by exposure to DCZ (**Extended Data Fig. 4d-g**).
159
160 Additionally, we performed a cFOS analysis in the $PBN_L$ of mice that received a colon balloon
161 placement either as a sham, or with a pressure distension of 80 mmHg to identify central
162 visceral pain-activated neurons. We found a substantial increase of cFOS-positive neurons in
163 $PBN_L$ following 30-min of stimuli and that the signal was significantly reduced by
164 chemogenetic silencing of the Nav1.8-lineage neurons (**Extended Data Fig. 4h,i**), suggesting
165 that peripheral Nav1.8$^+$ nociceptors are the active driver of visceral pain hypersensitivity and
166 trigger transmission of visceral pain signals into the central nervous system (CNS) to generate
167 adaptive behavioral responses.
168
169 **<u>Colitis drives a $PBN_L$ neural activation mediated by peripheral nociceptors and</u>**

170 **inflammation**

171 Neurons in the mouse parabrachial nucleus are molecularly diverse with multiple subsets of
172 cell types that reside within distinct spatial niches[20-22]. We performed activity-dependent
173 mapping in PBN neurons using cFOS expression to determine the neural activation pattern
174 along the $PBN_L$, a critical hub that receives multiple afferent inputs from the periphery and
175 projects to the brain to generate sensory and affective responses. Following the 4-day DSS
176 colitis induction paradigm we observed a significant increase in cFOS-positive signals in the
177 $PBN_L$ region compared to regular $H_2O$ controls (**Fig. 2a-c**). To verify whether this activation
178 in the $PBN_L$ is driven by primary sensory neurons, we utilized the Nav1.8-hM4Di mice for a
179 temporary chemogenetic silencing of nociceptors, and TRPV1-DTA mice for a selective
180 diphtheria toxin-based permanent ablation (DTA) of peripheral nociceptors. We observed a
181 considerable reduction of the colitis-induced cFOS activation following either temporary or
182 permanent silencing of Nav1.8 and TRPV1-lineage neurons, respectively (**Fig. 2a-f**).

183

184 To selectively capture neurons activated during DSS-induced colitis, we employed an activity-
185 dependent genetic labeling strategy by crossing TRAP2 mice with Rosa-lxl-tdTomato reporter
186 mice. TRAP2-tdTom mice were subjected to 4-day DSS treatment followed by an
187 administration of 4-hydroxytamoxifen (4-OHT). This approach enabled permanent labeling of
188 FOS-expressing neurons that were active during the defined colitis window, allowing
189 identification and analysis of DSS colitis-activated neuronal populations (**Fig. 2g**). We
190 observed a comparable increase in the tdTomato-positive signal relative to baseline as the
191 cFOS staining, and this increased FOS-driven activation was noticeably diminished in mice
192 that received ketorolac injections, a nonsteroidal anti-inflammatory drug, to dampen the DSS-
193 induced local inflammation in the colon (**Fig. 2h-i**). These results indicate that the central
194 activation of $PBN_L$ neurons is driven by peripheral inflammation and nociceptor inputs.

195

196 **$PBN^{colitis}$ neurons tune abdominal sensitivity**

197 Next, we sought to probe what function the activated $PBN_L$ ensemble may have in mediating
198 colitis pain and its associated affective phenotypes. To gain functional access to the cFOS-
199 driven population, we utilized TRAP2 mice to functionally label the colitis-activated neural
200 population. The TRAP2 mice first received a stereotaxic injection of AAVs encoded with Cre-
201 dependent DREADDS bilaterally into $PBN_L$. Colitis-activated $PBN_L$ ($PBN^{colitis}$) neurons were
202 tagged by treating the mice with DSS water followed by an injection of 4-OHT to induce iCre
203 recombination specifically in the FOS-expressing population (**Fig. 2j**). Quantification of the

204 signal overlap between TRAPed and FOS-positive cells induced by DSS colitis revealed a
205 ~60% TRAPing efficiency for the TRAPed and FOS-positive population (**Fig. 2k-m**). We then
206 asked whether $PBN^{colitis}$ neuronal activity is sufficient to modulate basal mechanical thresholds
207 in the abdominal region, a measure of the referred cutaneous hypersensitivity associated with
208 visceral pain (**Extended Data Fig. 5a**). We found that chemogenetic silencing (hM4Di) or
209 activation (hM3Dq) of the $PBN^{colitis}$ neurons bidirectionally tuned abdominal mechanical
210 sensitivity across a range of von Frey forces following DCZ administration when compared
211 with vehicle controls (**Extended Data Fig. 5b,d**).
212
213 When the same cohort of mice was assessed for basal hindpaw mechanical sensitivity, neither
214 silencing nor activation of $PBN^{colitis}$ neurons produced any observable change in the paw
215 withdrawal responses (**Extended Data Fig. 5c,e**). Hindpaw zymosan-activated $PBN_L$
216 ($PBN^{Zymosan}$) neurons modified the paw withdrawal response to von Frey stimuli (**Extended**
217 **Data Fig. 7a,b**) and thermal sensitivity and preference across a temperature gradient
218 (**Extended Data Fig. 7d-f**), but displayed a negligible modulatory effect on abdominal
219 sensitivity (**Extended Data Fig. 7c**). These results support a modality-specific role of the $PBN_L$
220 in visceral versus somatic nociceptive processing.
221
222 **<u>$PBN^{colitis}$ neurons gate behavioral responses towards visceral nociception</u>**
223 To evaluate the impact of $PBN^{colitis}$ neural activity in modulating colon pain-associated
224 behaviors, TRAP2 mice with Cre-dependent inhibitory hM4Di AAVs received a colonic
225 infusion of 0.05% capsaicin to activate TRPV1-lineage nociceptors in the distal colon to initiate
226 pain (**Fig. 2o**). We identified several distinct spontaneous behaviors, including lower body
227 licking, jumping and adnominal squashing immediately following the low-dose colonic
228 capsaicin exposure compared to vehicle treated controls (**Fig. 2n**). These spontaneous behavior
229 bouts were effectively reduced by silencing of $PBN^{colitis}$ neurons with DCZ, as opposed to the
230 increase in behavior bouts in vehicle treated mice (**Fig. 2p**). In parallel, we identified the
231 development of tactile allodynia over the abdominal region in the colonic capsaicin-treated
232 mice and that mechanical threshold returned close to baseline in response to $PBN^{colitis}$ neural
233 silencing (**Fig. 2q**).
234
235 **<u>$PBN^{colitis}$ neurons promote aversive states</u>**
236 To assess whether $PBN^{colitis}$ neurons influence affective and motivational valences we
237 implemented a three-chamber task where mice were allowed to freely explore a completely

238 shielded chamber ("hidden zone") or an open chamber ("open zone"). We then performed a
239 conditioning paradigm by pairing the injection of DCZ in mice in the hidden zone, and vehicle
240 in the open zone, in a set of mice that had previously received a stereotaxic delivery of Cre-
241 dependent hM3Dq AAV for chemogenetic activation, or mCherry AAV as controls (**Extended**
242 **Data Fig. 6a**). Real-time tracking of the mouse trajectory demonstrated that $PBN^{colitis}$
243 activation drove an aversive response, as revealed by a robust reduction of the time spent in
244 the hidden zone when that chamber was paired with DCZ treatment during the conditioning
245 sessions (**Extended Data Fig. 6b,c**). In parallel, we also conducted a two-bottle choice test to
246 monitor motivational changes towards an appetitive incentive (**Extended Data Fig. 6d**) and
247 found that a strong taste aversion developed in mice after $PBN^{colitis}$ activation conditioning, as
248 indicated by significantly reduced consumption of sucrose when paired with DCZ treatment,
249 compared with the control group (**Extended Data Fig. 6e,f**).
250
251 **<u>$PBN_L$ neurotensin neurons encode visceral pain induced by colonic insults</u>**
252 Cell type-specific populations reside in different subregions of the $PBN_L$ and form distinct
253 projection patterns and circuit functions[12,21,32]. We divided colonic stimulation induced cFOS
254 expression in the $PBN_L$ region into two distinct subregions, the external lateral PBN (elPBN)
255 and the dorsal lateral PBN (dlPBN), based on established anatomical boundary standards[12,20,21].
256 We identified enriched cFOS-positive signals within the elPBN region following DSS-induced
257 colitis, which comprised ~67.5% of cFOS-positive signals within the elPBN compared to
258 ~32.5% within the dlPBN (**Extended Data Fig. 8**), indicating preferential activation of neural
259 ensembles within elPBN under the condition of colitis. We then focused on the elPBN
260 subregion to identify the neuronal cell types recruited during colitis using an established spatial
261 transcriptomic dataset[20,21]. The elPBN region primarily encompasses a *Calca*-expressing
262 population along with other gene markers, including *Tac1*, *Penk*, *Crh and Nts*. To focus on
263 those elPBN neurons that send projections to sensory and pain-regulating brain regions, we
264 used *Crh* and *Nts* markers to evaluate signal overlap in our cFOS dataset. We collected $PBN_L$
265 from mice that had either received 3% DSS drinking water for 4 days to induce colitis or 20
266 μL of 5 mg/mL zymosan into the left hindpaw for 6 hours to induce plantar skin inflammation[33]
267 (**Fig. 3a**). We determined the signal overlap between the two marker genes and *Fos* expression
268 by performing RNAscope on serial sections of $PBN_L$ (**Fig. 3b**). $Nts^+$ neurons displayed a ~65%
269 overlap with $Fos^+$ signals in neurons during DSS colitis, with only a ~30% signal overlap with
270 $Crh^+$ neurons, and a ~25% overlap between $Nts^+$ and $Fos^+$ signals in neurons following
271 hindpaw zymosan (**Fig. 3c**), suggesting a preferential role of neurotensin-expressing $PBN_L$

272 neurons in encoding visceral over somatic pain.
273
274 Using a neurotensin genetic driver of Cre mice (NT-Cre), we next sought to delineate the *in*
275 *vivo* calcium dynamics of the $PBN_L$ NT neurons using fiber photometry in response to the
276 visceral pain elicited by noxious distension with a pressurized colon balloon (**Fig. 3d-f**). We
277 inserted a balloon with a bifurcated ending to an air-pressured syringe and a manometer to
278 monitor balloon distension pressure within the colon simultaneously (**Fig. 3d**) and introduced
279 pressures of 20, 40 and 80 mmHg into the balloon to mechanically distend the colonic lumen
280 with a 5-sec inflation to the designated pressure and a 5-sec deflation back to the baseline
281 pressure. We observed an encoding of the $PBN_L$ NT neural population to colonic distension in
282 a pressure intensity-dependent manner (**Fig. 3g-i**), providing direct evidence for their role in
283 the central processing of visceral afferent insults.
284
285 **<u>$PBN_L$ neurotensin neurons control visceral reflex and behavioral responses to colonic</u>**
286 **<u>insults</u>**
287 We next sought to determine whether central NT-positive neurons play a functional role in
288 colitis-induced symptoms. We utilized two different AAV-based silencing strategies to explore
289 the impact of reduced $PBN_L$ NT activity on the aberrant behavior and altered GI function
290 triggered by DSS-colitis. We injected an AAV vector that encoded (1) Cre-dependent hM4Di
291 (2) Cre-dependent TeLC (tetanus toxin light chain) or (3) Cre-dependent GFP into the bilateral
292 $PBN_L$ of NT-Cre mice and evaluated behavioral outcomes over a 4-day DSS treatment regimen
293 (**Fig. 4a-c**). Temporary silencing elicited by M4 muscarinic receptor binding to the DREADD
294 agonist versus long-term silencing mediated by a tetanus toxin-based synaptic blockade were
295 implemented to compare their analgesic profiles on colitis-induced licking behavior (**Fig. 4d**).
296 We found a robust attenuation of nociceptive licking behavior in mice that received 0.1 mg/kg
297 of DCZ (once per day for 4 days) to silence $PBN_L$ NT activity during DSS treatment, and that
298 this analgesic effect persisted beyond the chemogenetic silencing period when compared to the
299 GFP control group (**Fig. 4e**). Long-term silencing of NT release in the $PBN_L$ by tetanus toxin
300 substantially reduced the colitis-induced licking behavior with only a marginal increase in
301 licking bouts at D7 (**Fig. 4e**).
302
303 Licking bouts in mice are modulated either by a local inflammation-induced sensitization
304 driven by Nav1.8-lineage nociceptors or through a body-axis projection that controls
305 gastrointestinal (GI) physiology[34,35]. To test whether central NT neural activity modulates GI

306 function, we delivered DCZ to NT-Cre mice that had received a Cre-dependent hM4Di or GFP
307 AAV in the $PBN_L$ during the DSS treatment, followed by an oral gavage of carmine dye at D7
308 to measure gastrointestinal transit time (**Fig. 4f**). In the NT-silenced group we found a
309 normalization of the colitis-accelerated gut motility, as revealed by cumulative stool number
310 over time and the latency to the first red fecal pellet expelled by the mice (**Fig. 4g,h**). We
311 measured local colon sensitivity in response to a series of controlled distensions using a close-
312 loop balloon barostat device in both the NT-silenced and control groups (**Fig. 4i**). Distension
313 intensity-dependent changes of the colon reflex were present in control mice, with a large
314 increase of the response when the distension pressure surpassed 60 mmHg. Importantly, these
315 evoked responses were largely dampened in NT-silenced mice (**Fig. 4j,k**). We conclude that
316 $PBN_L$ NT neurons serve as a central hub to both sense visceral hypersensitivity and impact
317 associated colonic reflex and behavioral outputs.
318
319 **<u>$PBN_L$ neurotensin neurons protect against colitis-induced pathology</u>**
320 To determine whether silencing $PBN_L$ NT neurons attenuate the histopathological outcomes of
321 DSS-induced inflammation, we administered a calibrated dose of DCZ into the mouse drinking
322 water to achieve a sustained silencing of $PBN_L$ NT neurons that matches the multi-day
323 progression of the pathology (**Extended Data Fig. 10a**). Longitudinal assessment of the stool-
324 based disease activity index (DAI) revealed that chronic NT-silencing significantly improved
325 stool consistency and fecal bleeding, and reduced DAI compared to a non-silenced control
326 group, as the disease progressed toward D7 (**Extended Data Fig. 10b**). Analysis of the colon
327 revealed that silencing $PBN_L$ NT neurons reduced neutrophil infiltration and preserved crypt
328 integrity and overall colon length (**Extended Data Fig. 10c-e**). Fecal lipocalin-2, an
329 inflammatory marker of mucosal immune activation, was significantly elevated at D7 under
330 DSS colitis but was markedly reduced in the NT-silencing group (**Extended Data Fig. 10h**).
331 These protective effects appeared to occur independently of overt systemic immune alterations,
332 as evidenced by a lack of weight change in spleen and mesenteric lymph nodes (**Extended**
333 **Data Fig. 10f,g**). These data indicate that $PBN_L$ NT neurons can exert a protective influence
334 against colitis-mediated pathology.
335
336 **<u>$PBN_L$ neurotensin neurons exert a restricted modulation of somatic inflammatory pain</u>**
337 We next investigated whether $PBN_L$ NT neurons differentially modulate distinct peripheral
338 sensory modalities. An intraplantar injection of zymosan was administered to induce
339 inflammatory pain in the hindpaw. Somatic hypersensitivity was analyzed by measuring

340 contact luminance of the hindpaws via a transillumination recording platform[30]. A reduction in
341 contact luminance is a proxy for tactile allodynia as zymosan-induced inflammation reduces
342 plantar surface contact (**Extended Data Fig. 9a,b**). Contrary to the effects observed in the
343 colitis model, silencing of $PBN_L$ NT neurons did not significantly attenuate the zymosan-
344 induced hypersensitivity throughout the three-day post-injection period (**Extended Data Fig.**
345 **9c**).
346
347 **Blocking neurotensin signaling attenuates colitis-induced pain-related behavior**
348 We next aimed to investigate the downstream brain targets that receive neural projections from
349 the $PBN_L$ NT neurons by conducting an AAV-based projection mapping, and identified several
350 regions known to regulate pain, including the bed nucleus of the stria terminalis (BNST),
351 central amygdala (CeA), ventral posteromedial (VM) thalamus and dorsolateral periaqueductal
352 gray (dlPAG) (**Extended Data Fig. 11a**). We then evaluated whether blockade of downstream
353 terminal NT release could provide any therapeutic relief of colitis-associated pain-related
354 behaviors. To confirm a functional connectivity between colitis-activated $PBN_L$ neurons and
355 the terminal release of NT in the CeA, we delivered a Cre-dependent hM3Dq into the $PBN_L$
356 region of TRAP2-Cre mice, followed by a 4-OHT injection during the 4-day DSS treatment to
357 induce the labeling of $PB^{colitis}$ by a FOS driver (**Extended Data Fig. 11b**). In the CeA, we
358 delivered a G protein–coupled receptor activation–based neurotensin sensor (GRAB-NT1.0)[36]
359 followed by an optic fiber implant to monitor NT release dynamics *in vivo* (**Extended Data**
360 **Fig. 11c**). We detected a robust surge in NT release in the CeA region after activation of $PB^{colitis}$
361 by DCZ treatment, as compared to the baseline signal in the vehicle treatment group (**Extended**
362 **Data Fig. 11d,e**), confirming NT signaling in the PBN-CeA pathway. To test whether blocking
363 neurotensin receptor type 1 (NTSR1) signaling in the CeA region affects DSS-colitis
364 behaviors, we implanted cannulas bilaterally in the CeA for selective NTSR1 antagonist,
365 SR48692, infusions (0.3 μL/day at 20 nM) over 4-day DSS treatment (**Extended Data Fig.**
366 **11f**). This produced an effective attenuation of colitis-induced licking behavior bouts as well
367 as a reduction in diarrhea, as evidenced by the normalization of the stool water content
368 (**Extended Data Fig. 11g-i**). These results highlight CNS neurotensin signaling as a key
369 modulator that calibrates colitis-induced visceral pain and associated gastrointestinal
370 pathological changes.
371
372 **Discussion**

373 Understanding the central neural modules that encode and regulate visceral sensation has been
374 hindered by the diffuse and heterogeneous nature of the peripheral innervation of viscera and
375 the absence of robust pain-related behavioral reflexes that allow direct functional
376 assessment[4,6,37]. We implemented a supervised machine-learning framework that integrates
377 pose estimation with body-part contact detection to extract subtle and disease-relevant
378 behaviors. We identified a distinct lower body licking behavior that emerged selectively in
379 mice with colitis. Notably, this behavioral signature closely tracked the temporal dynamics of
380 the colonic inflammation and was functionally dependent on Nav1.8-lineage nociceptors.
381
382 By combining FOS-based activity mapping with TRAP to identify activation-defined neuronal
383 populations, we found that DSS-induced colitis preferentially recruits neurons within the
384 external lateral PBN, a region implicated in encoding aversive salience and the affective
385 valuation of bodily threat[13,24,38]. Silencing this colitis-activated parabrachial ensemble
386 ($PBN^{colitis}$) markedly attenuated the behavioral responses to an acute intracolonic capsaicin
387 challenge. In contrast to somatosensory pain, visceral pain is commonly characterized by
388 emotional distress and is therefore thought to substantially engage limbic and affective
389 circuits[39]. Consistent with this, we found that activation of $PBN^{colitis}$ neurons robustly drives
390 aversive behavior as assessed by both conditioned place and conditioned taste paradigms,
391 indicating that this neural ensemble engaged during visceral inflammation promotes a negative
392 valence.
393
394 The enrichment of FOS-positive neurons within the elPBN in response to colitis prompted us
395 to define the molecular identity of the colitis-responsive cell types in this region. We
396 discovered that neurotensin-expressing neurons exhibited a selective overlap with colitis-
397 induced FOS activation, with minimal overlap with the FOS signals elicited by a zymosan-
398 induced somatic inflammation in the hindpaw, supporting preferential engagement of the $PBN_L$
399 NT population by visceral rather than somatic afferent inputs. Using *in vivo* fiber photometric
400 recordings, we further demonstrated that $PBN_L$ NT ensemble activity increased robustly in
401 response to graded colorectal distension when intraluminal distension exceeded 40 mmHg.
402 This threshold-dependent profile parallels the force-response characteristics observed in most
403 colon-innervating dorsal root ganglion neuron subtypes[40,41], supporting the notion that $PBN_L$
404 NT neurons encode high-threshold visceral nociceptive signals.
405

406 $PBN_L$ NT neurons constitute a distinct subset of the excitatory population within the elPBN
407 region and partially overlap with *Calca*, *Oprm1* and *Tac1* markers, which have been implicated
408 in pain modulation. We found that silencing the $PBN_L$ NT population, using either
409 chemogenetics, or toxin-directed impairment of synaptic transmission, generated a profound
410 analgesic effect, as evidenced by a marked reduction in colitis-associated licking behavior.
411 Notably, this analgesic effect was more sustained than that achieved by targeting Nav1.8-
412 lineage nociceptors, indicating that $PBN_L$ NT neurons operate at a higher-order integrative
413 node in the visceral pain pathway. We reasoned that the improvement of the nocifensive
414 behavior is contributed by a normalization of local hypersensitivity in the sensitized colon.
415 Importantly, we identified a significant reduction in the colonic hyperreflex triggered by
416 barostat distension with $PBN_L$ NT silencing, particularly at pressures exceeding the 40 mmHg
417 threshold associated with visceral pain. In addition, $PBN_L$ NT silencing also restored
418 gastrointestinal transit, emphasizing that this neuronal population integrates visceral sensory
419 inputs to coordinate both pain-related behaviors and peripheral organ-level physiological
420 responses.
421
422 Neurotensin has been implicated in the regulation of fundamental homeostatic processes,
423 including feeding, social valence and pain[42-44], and has also been characterized as a peripheral
424 proinflammatory mediator, as evidenced by an elevated expression of its receptor, NTSR1 in
425 the colon in experimental colitis models[45-47]. We hypothesized that central neurotensin
426 signaling contributes to the visceral nociceptive and autonomic sequelae of colitis. Using
427 AAV-based circuit tracing, we revealed that $PBN_L$ NT neurons project to affective brain
428 regions, with a particularly dense innervation of the central amygdala (CeA). Activation of this
429 parabrachial source evoked a robust surge in NT release in the CeA, as detected by a
430 neurotensin-based GRAB sensor. Importantly, pharmacological blockade of NTSR1 signaling
431 within the CeA effectively ameliorated colitis-associated licking behavior and diarrhea,
432 indicating that central NT signaling acts as a supraspinal modulator of disease severity,
433 potentially through the amplification of those aversive and autonomic pathways that feed back
434 onto peripheral visceral inflammatory and nociceptive processes[34,35,48]. By integrating machine
435 learning-assisted behavioral decoding, molecular profiling, *in vivo* neural activity recording,
436 and circuit-specific manipulations, our study provides evidence for a central circuit mediated
437 modulation of peripheral visceral function. These findings offer a mechanistic framework for
438 understanding those visceral disorders arising from dysregulated brain-body interactions, and

439 pinpoint neurotensin in the CNS as a potential therapeutic target that can be leveraged to treat
440 colitis-induced visceral pain.
441
442 **Materials and Methods**
443 **Animals**
444 All animal husbandry and procedures involving mice were conducted in strict accordance with
445 guidelines set forth by the Boston Children's Hospital Institutional Animal Use and Care
446 Committee. Mice at 6-8 weeks of age with the strains of C57BL/6J (B6, JAX #000664), $Fos^{2A-}$
447 $^{iCreER}$ (TRAP2, JAX #030323), Nav1.8-Cre (JAX #036564), NT-Cre (JAX #017525), R26-
448 LSL-hM4Di/mCitrine (JAX #026219), Ai14(RCL-tdTomato)-D (JAX #007914), TRPV1-Cre
449 (JAX #017769) and ROSA-DTA (JAX #009669) were obtained from the Jackson Laboratory.
450 Adult mice of 8-12 weeks of age for both male and female mice of heterozygous alleles were
451 used for this study. Induction of iCre-mediated recombination in the TRAP2 mice was
452 performed by an i.p. injection of 0.1 mL of 10 mg/mL of 4-OHT dissolved in corn oil, with
453 experiments beginning ~2 weeks after the induction.
454
455 **Pharmacological reagents**
456 Dextran sulfate sodium salt (MP Biomedicals #0216011080) was dissolved in regular drinking
457 water at a concentration of 3% to induce colitis, 4-hydroxytamoxifen (Sigma-Aldrich #H6278)
458 was prepared in corn oil and ethanol for the induction of $Cre^{ER}$ translocation,
459 deschloroclozapine (Hello Bio #HB9126) was prepared in saline solution as an agonist for
460 DREADDs experiments, ketorolac (TargetMol #T1212) was prepared in saline, capsaicin
461 (Tocris #0462) was dissolved in ethanol, tween80 and saline to induce acute nociceptive
462 responses, zymosan A from saccharomyces cerevisiae (Sigma-Aldrich #Z4250) was prepared
463 in saline solution for intraplantar injection to induce hindpaw inflammation and pain. SR48692
464 (Sigma-Aldrich #SML0278), a selective NTSR1 antagonist, was prepared at 20 nM in a
465 solution of saline with 2% dimethylsulfoxide (DMSO). Carmine powder (Sigma-Aldrich
466 #C1022) was prepared at 6% w/v with methylcellulose to measure gut transit time.
467
468 **Adeno-associated virus (AAV) reagents**
469 For chemogenetic manipulation of $PBN_L$ neurons the following AAV vectors were used:
470 AAV2/1-hSyn-DIO-hM4Di-mCherry (BCH Viral Core; $3.51\times10^{13}$ gc/mL) for silencing,
471 AAV2/1-hSyn-DIO-hM3Dq-mCherry (BCH Viral Core; $2\times10^{13}$ gc/mL) for activation and
472 AAV2/1-hSyn-DIO-mCherry (BCH Viral Core; $3.48\times10^{13}$ gc/mL) as fluorescent controls. For

473 permanent silencing of $PBN_L$ neurons AAV2/8-hSyn-FLEX-TeLC-GFP (BCH Viral Core;
474 $1.56\times10^{13}$ gc/mL) was used to block synaptic transmission. For fiber photometric recording
475 AAV2/8-hSyn-FLEX-jGCaMP8s-WPRE (BCH Viral Core; $4.16\times10^{13}$ gc/mL) was used to
476 monitor neural calcium activity and AAV2/1-hSyn-FLEX-H2b-GFP (BCH Viral Core; $3\times10^{13}$
477 gc/mL) for fluorescent controls. To detect neurotensin release AAV2/1-hSyn-GRAB-NT1.0
478 (Addgene plasmid #180006 from Y. Li, viral vector packaged by BCH Viral Core; $2.78\times10^{13}$
479 gc/mL) was used.
480
481 **Stereotaxic injections and surgical procedures**
482 *Intracranial AAV vector injections*
483 Intracranial injections were conducted with aseptic procedures on a digital stereotaxic platform
484 for small animals. Mice were anesthetized with 4% isoflurane and maintained with ~1.5%
485 throughout the entire surgery on a feedback-controlled heating pad at a body temperature of
486 ~37°C. We injected AAVs using a 33 gauge, 5 µL microsyringe (Hamilton #65460-03) at a
487 rate of 50 nL/min for 250 nL volume in one injection site. $PBN_L$ was targeted at coordinates
488 relative to bregma: AP= –5.20 mm, ML= ±1.43 mm, DV= –3.55 mm. CeA was targeted at
489 coordinates: AP= 1.15 mm, ML= ±2.83 mm, DV= −4.17 mm. Mice were allowed to recover
490 and waited for at least 3 weeks for the virus to express before experiments were conducted.
491 *Optic fiber and cannula implantation*
492 The optic fiber was placed ~0.3 mm above the AAV injection site to monitor bulk calcium
493 activity using fiber photometric recording. For pharmacological experiments, cannulae (22GA,
494 PlasticsOne) were implanted bilaterally above the targeted brain region for repeated infusions
495 of drug into the mouse brain. All implants were tightly anchored onto the skull and secured
496 with Metabond (Parkell) and dental cement. Implanted mice were allowed to recover at least 2
497 weeks before experiments.
498
499 **Behavior assays**
500 *Spontaneous behavior recording*
501 Mice were individually placed in a 18 × 18 × 15 cm (length x width x height) black acrylic
502 chamber closed on all sides (BlackBox Bio) except for an NIR camera (Basler acA2000-
503 50gmNIR GigE, Basler AG, Ahrensburg, Germany) was positioned 30 cm beneath the glass
504 surface to track whole body movement from a bottom-up perspective[30]. Image brightness
505 features were captured using LED light reflected changes in pixel intensity acquired at a frame
506 rate of 25 Hz with 1000 × 1000 pixels dimensions. Mice were habituated in the recording

507 chamber 1 hour per day for three days before the start of the experiment. Recordings were
508 performed in both experiment and control groups on the same day for 30 min in each session
509 during the animal's light cycle.

510 Automated behavior screening

511 Lower body licking behavior was quantified using BAREfoot, a supervised machine learning
512 framework that integrates pose estimation with light-based measurements of body-part
513 pressure and spatial distance[29]. Training datasets for the lower body licking classifier were
514 generated through manual annotation of video recordings by experienced scorers, after which
515 new classifiers were trained on these labeled data. After testing and validating classifier
516 performance, automated detection and quantification of lower body licking behaviors bouts
517 was performed. Manual annotation of spontaneous behavior signatures, including peri-anal
518 licking (repetitive licking around the anal port), abdomen licking (repetitive licking on a fixed
519 region of the lower abdomen), abdomen squashing (contact with pressing of the lower abdomen
520 against the floor), hunching (shortening the distance between fore and hindlimbs) and jumping
521 (leaping off the floor with two hindlimbs), were labeled by three experienced independent
522 investigators on a frame-by-frame level using a customized MATLAB scoring platform.

523 *Paw luminance measurement*

524 Hind paw coordinates were tracked using DeepLabCut[49], and 23 × 23 squared pixels centered
525 on these locations were extracted from the FTIR frames. Tactile allodynia was assessed by
526 measuring paw luminance, defined as the average pixel brightness within each extracted ROI.

527 *Abdominal and plantar von Frey assay*

528 Mice were habituated in von Frey chambers on a meshed floor for three days (1 hour per day),
529 including the day of the test, before the mechanical sensitivity was evaluated. To evaluate the
530 reflexive sensitivity in response to mechanical stimuli, a logarithmically increasing set of 8 von
531 Frey filaments (Stoelting Co, #58011) ranging from 0.02 to 4.0 grams were applied
532 perpendicularly to the plantar hindpaw or lower abdomen with a sufficient force to gently bend
533 the monofilament. We employed the up-down method to measure the 50% withdrawal
534 threshold on the mice lower abdomen or plantar hindpaw[50]. The response frequency was
535 measured as the number of positive rapid withdrawal of the lower abdominal region or the
536 hindpaw in response to 10 von Frey stimulations at an interval of at least 30 sec between each
537 stimulus. All the behavior tests were conducted in a blinded fashion to either the experimental
538 vs control group, or the injection of treatment vs vehicle group.

539 *Colorectal distension*

540 Mice were briefly anesthetized with ~1.5% of isoflurane to receive a lubricated polyethylene
541 balloon insertion through the rectal port as previously described[51]. A colonic balloon with a
542 diameter of ~2 mm was gently placed at the distal colon segment ~20 mm from the mouse anal
543 verge and connected to a pressure-equalization tubing with a manometer (Cole Parmer)
544 positioned at the bifurcation to simultaneously monitor distension pressure. A pressured tape
545 was attached to the base of the tail to secure the placement of the colonic balloon for freely
546 behavior recording. For each distension trial, the balloon was inflated to the designated
547 pressure of 40 mmHg or 80 mm Hg within 5 seconds and a 5-sec deflation back to the baseline
548 pressure for a total of 30-sec distension. Each behavioral recording consisted of alternation of
549 30-second distension and 30-second rest, continuously over a 30-minute recording session.
550 *Conditioned motivation tests*
551 To evaluate the impact of colitis-activated $PBN_L$ neurons on motivational behaviors in mice,
552 we conducted conditioned place motivation and conditioned taste motivation tasks. For
553 conditioned place motivation, mice were habituated for 1 hour in a three-chamber apparatus
554 separated with a central corridor that allowed free access to left or right compartment, including
555 one shielded compartment with a meshed floor (hidden zone) and the other open compartment
556 with a smooth acrylic floor (open zone). On day 1, mice were placed in the central corridor to
557 freely explore both compartments for 30 min to determine the place preference by tracking the
558 time spent across the entire apparatus using Ethovision XT (Noldus). On conditioning day 2
559 and 3, mice were confined to each compartment and paired with an i.p. injection of 0.1 mg/kg
560 DCZ in the hidden zone, or vehicle in the open zone for 1 hour. The conditioning occurred
561 twice a day (9 AM and 5 PM) with alternating compartments for a period of 2 days. On day 4,
562 mice were re-introduced back into the central corridor to freely explore for 30 min to record
563 the time spent in each compartment. For conditioned taste motivation, mice were single-housed
564 and habituated to the home cages and water bottles for three days before the experiment. Prior
565 to each day of conditioning, mice were restricted to water access overnight and the
566 consumption amount was measured during the light cycle (9 AM to 5 PM). On day 1 and day
567 3, mice were allowed to have free access to regular drinking water in the home cage for 30
568 min, followed by an i.p. injection of vehicle, then returned to the home cage until 8 hours were
569 timed to measure the consumption amount of solution. On day 2 and day 4, mice were given
570 free access to a 10% sucrose solution in the water bottle for 30 min, followed by an i.p. injection
571 of 0.1 mg/kg DCZ, then returned to the home cage until 8 hours were timed. On day 5, mice
572 were given two bottles that contained regular water and 10% sucrose in each, for 8 hours to

measure the taste preference. The preference index of sucrose over water during the two-bottle test on day 5: (amount of sucrose consumption) / (amount of water + sucrose consumption).

*Thermal gradient ring (TGR)*

Mice were habituated for 30 min in the thermal gradient ring (Ugo Basile #35550) with the platform temperature pre-set to 10°C on one side and 55°C on the opposite side at an increment of 5°C along the circular ring. During the test, each mouse was allowed to freely explore along the TGR setup for 1 hour and the occupancy duration as well as distance traveled in each temperature zone were recorded using the ANY MAZE software.

*Hotplate assay*

Thermal nociceptive thresholds were assessed using a hotplate assay. Mice were first acclimated to the device for 1 hour before the experiment. The hotplate (BIOSEB) was preset and maintained at a constant temperature of 52°C degree. Each mouse was placed within a transparent plexiglas cylinder on the heated surface, and the latency to exhibit the first nocifensive flinching behavior was recorded. A maximum cut-off time of 30 seconds was implemented to prevent plantar damage. Each mouse was tested in three trials with at least 10-minute between trials and the average latency is calculated.

*Gastrointestinal (GI) transit assay*

To assess total gastrointestinal transit time, mice were orally gavaged 300 μL of 6% carmine red powder dissolved in 0.5% methylcellulose as previously described method[52]. Mice were then placed individually in clean home cages to measure the number of expelled stools. The GI transit time was defined as the interval between oral gavage and the first observation of a carmine-colored fecal pellet with the observation conducted every 10 minutes to ensure temporal accuracy.

**Physiological recordings**

*In vivo fiber photometry recording in awake behaving mice*

Optical fibers (400 μm core diameter, RWD) were implanted two weeks following Cre-dependent AAV delivery of GCaMP8s or GRAB-NT1.0. During implantation, real-time photometric signals were monitored to optimize fiber placement depth to maximize fluorescence signal intensity. Photometric recordings were acquired using a fiber photometry system (Doric Lenses) controlled by Doric Neuroscience Studio software. Excitation light at 405 nm (isosbestic, activity-independent control) and 465 nm (activity-dependent signal) was delivered, and emitted fluorescence signals were recorded at a sampling rate of 120 Hz. To enable temporal alignment with behavioral recordings, the fiber photometry system generated

607 a synchronization light pulse every 90 s, which was captured concurrently by a behavior video
608 camera operating at 30 Hz. Raw photometry signals were processed by averaging every 12
609 consecutive samples, yielding an effective sampling rate of 10 Hz. To directly compare neural
610 activity and behavior response to stimulus onset, fiber photometry and video-derived
611 behavioral signals were resampled onto a shared time base. Photometry data were exported to
612 MATLAB (MathWorks) for further processing and analysis. Fluorescence signals were
613 expressed as $\Delta F/F$, calculated as $\Delta F/F = (F - F_0)/F_0$, where F represents the 465 nm activity-
614 dependent signal and $F_0$ denotes the fitted isosbestic control signal derived from the 405 nm
615 channel. Z-scored $\Delta F/F$ values were used for synchronization and subsequent analyses.
616 *Distension barostat recording*
617 For assessment of colonic sensitivity, colorectal distension was performed using a close-loop,
618 programmed balloon distension barostat (G&J Electronics Inc). Mice were briefly anesthetized
619 with 3% isoflurane followed by an i.p. injection of either vehicle or DCZ. Mice were then
620 loosely positioned in a cylindrical restrainer, and a lubricated flexible balloon catheter was
621 gently guided into the anus and advanced into the distal colon. The catheter was secured by
622 taping it to the tail and the restrainer was tightened to minimize movement. Mice were allowed
623 to recover fully from anesthesia and habituate in the restrainer for 30 min prior to recording
624 experiment. The barostat operated through a closed-loop feedback system and utilized an
625 internal pressure transducer to monitor intracolonic pressure change in real-time. The
626 distension protocol is consisted of balloon inflation to graded pressures of 20, 40, 60, and 80
627 mmHg for 10 sec per distension pressure, with a 3-min inter-stimulus interval between
628 distensions. Each pressure series was repeated three times. The barostat control signal
629 indicating balloon distension was synchronized with the intracolonic pressure recordings
630 obtained from the probe sensor to define distension timing and pressure levels. All raw data
631 were acquired and processed using LabChart software (ADInstruments). To isolate dynamic
632 pressure fluctuations, the intracolonic pressure signal was processed offline using a high-pass
633 Butterworth filter (cutoff frequency, 0.1 Hz) to remove low-frequency background drift. The
634 root mean square (RMS) amplitude of the filtered signal was calculated within predefined
635 analysis windows and stored as a derived signal. For each distension epoch, the area under
636 curve (AUC) of the RMS signal was calculated relative to the pre-distension baseline and used
637 as an integrated measure of intracolonic pressure activity. Identical filtering parameters and
638 analysis windows were applied across all experimental sessions.
639
640 **Colon histopathology and stool composition analyses**

641 *Colitis severity evaluation*

642 Colon tissues were prepared as swiss-rolls, fixed, and sectioned for Hematoxylin & Eosin
643 (H&E) staining to assess the severity of colonic inflammation. Colitis severity was assessed
644 using a semi-quantitative scoring system based on three parameters: crypt dropout, submucosal
645 expansion, and neutrophil infiltration. Each parameter was scored on a scale from 0 to 3, where
646 0 represented absence of pathology and 3 indicated severe involvement. The scores from all
647 three parameters were summed to yield a total histology score ranging from 0 to 9, with higher
648 scores reflecting greater tissue damage and inflammatory severity. Disease activity was further
649 assessed using a stool-based disease activity index (DAI), which was calculated as the sum of
650 two components: stool consistency and fecal blood. Stool consistency was scored as follows:
651 formed and soft=1, loose or semi-formed=2, diarrhea=3. Fecal blood was evaluated using a
652 Hemoccult card (Beckman Coulter) to detect occult blood and scored as follows: occult
653 blood=1, visible blood=2, rectal bleeding=3. For stool composition measurements, mice were
654 transferred to clean cages and allowed free access to food and water. Stool output was
655 continuously collected for 1 h. The total mass of fecal material collected during this period was
656 recorded as the wet weight per mouse. Collected fecal pellets were then air-dried for 14 days
657 until a stable mass was achieved, at which point the dry weight was recorded. Percentage of
658 fecal water content = [(wet−dry)/wet]x100.

659 *Fecal lipocalin-2 (LCN2/NGAL) quantification by ELISA*

660 Fecal lipocalin-2 levels were quantified using a sandwich ELISA (DuoSet™ Mouse Lipocalin-
661 2/NGAL, R&D Systems/Bio-Techne; DY1857) according to the manufacturer's instructions.
662 Frozen fecal pellets were weighed and resuspended at 100 mg/mL in PBS containing 0.1%
663 Tween-20, vigorously homogenized by vortexing, and clarified by centrifugation at maximum
664 speed for 1 min. The resulting supernatant was collected, stored at −80 °C, and subsequently
665 used for ELISA analysis.

666

667 **Immunohistochemistry**

668 Mice were anesthetized with an i.p. injection of 200 mg/kg pentobarbital and perfused
669 transcardially with an ice-cold 1xPBS, followed by 4% paraformaldehyde (PFA) in 1xPBS.
670 The brain, DRG and colon tissues were post-fixed for 4-6 hrs at 4°C and transferred to 30%
671 sucrose in 1xPBS for 2 days. Tissues were frozen in O.C.T. (Tissue-Tek) and sectioned with a
672 cryostat at 40-µm thickness. Sliced tissues were mounted on histology slides and immersed in
673 blocking solution containing 5% normal donkey or goat serum and 0.3% Triton X-100 in
674 1xPBS for 1 hr at 4°C. The tissue slides were then incubated with primary antibodies at 4°C

675 overnight. On the next day, tissues underwent extensive wash with clean 1xPBS followed by
676 incubation with appropriate secondary antibody conjugated with AlexaFluor for 2 hrs at room
677 temperature. After washing with 1xPBS for 5 min three times, stained slides were coverslipped
678 with ProLong Diamond Antifade Mountant (Thermo Fisher, P36970). Histological images
679 were acquired using either a Leica SP8 or Zeiss LSM 980 confocal microscope at a resolution
680 of 1024 × 1024 pixels, using 10× or 20× air objectives with z-stack step sizes of 2–5 μm.
681 Immunofluorescence signals were quantified using ImageJ (NIH, v1.53f). For each histological
682 section, 8-10 consecutive z-slices were acquired and combined using an average-intensity z-
683 projection. Projected images were background-subtracted and thresholded to generate binary
684 masks of fluorescent signals. Automated particle/cell counting was performed to quantify the
685 number of detected fluorescent cells. The following primary antibodies were used: anti-cFOS
686 (Cell Signaling, #2250), anti-RFP (Rockland #48710), anti-Nav1.8 (Alamone Labs #ASC028),
687 anti-CD45 (eBioscience #14-0451-82), anti-GFP (Thermo Fisher #A10262); secondary
688 antibodies were used: Alexa Fluor™ 555-conjugated donkey anti-rabbit (Invitrogen #A31572),
689 Alexa Fluor™ 594-conjugated goat anti-rabbit (Invitrogen #A11012), Alexa Fluor™ 488-
690 conjugated goat anti-mouse (Invitrogen #A11001), Alexa Fluor™ 488-conjugated goat anti-
691 chicken (Invitrogen #A11039).
692
693 **Fluorescence in situ hybridization**
694 Mice underwent transcardial perfusion with 4% PFA and brains were post-fixed overnight and
695 30% sucrose for 48 hrs. Tissues were fresh-frozen in O.C.T. compound (Thermo Fisher
696 Scientific) and stored at −80 °C until cryoslicing. Coronal sections of 20 μm thickness covering
697 the entire PBN region were serially collected and mounted onto Superfrost Plus slides (Thermo
698 Fisher Scientific) and stored at −80 °C for processing. RNAscope in situ hybridization was
699 performed using the RNAscope Fluorescent Multiplex V2 Kit (Advanced Cell Diagnostics)
700 following the manufacturer's instructions. Slides were dehydrated through graded ethanol
701 (50%, 70%, and 100%) and treated with hydrogen peroxide for 10 min, washed, and incubated
702 with Protease IV for 30 min at room temperature. The following probes from Advanced Cell
703 Diagnostics were used: Mm-Fos (316921), Mm-Nts (420441) and Mm-Crh (316091). Sections
704 were incubated for probe hybridization and signal amplification steps in a HybEZ oven (ACD
705 Bio) at 40 °C. Fluorescent signal detection was achieved using TSA Plus HRP reagents and
706 Opal 520, 570, and 620 dyes (Akoya Biosciences). HRP reagents were applied for 15 min and
707 Opal dyes for 30 min at 40 °C with 15min HRP blocking steps between each channel and wash
708 buffer rinses between all incubations. FISH images covering serial sections of the $PBN_L$

709 between bregma −5.0 mm and −5.4 mm were analyzed using ImageJ. Image brightness and
710 contrast were adjusted using consistent thresholding parameters to optimize visualization of
711 each fluorophore. Cellular boundaries were defined based on DAPI labeling, and individual
712 mRNA puncta (5–10 pixels in diameter) were quantified within each cell. Cells containing >5
713 puncta of Fos, Nts, or Crh mRNA were classified as marker-positive. This threshold was
714 applied consistently across all analyzed sections to determine the overlapping of gene-
715 expressing populations.
716
717 **Statistical analysis**
718 All statistical analyses were performed using GraphPad Prism. The specific statistical tests
719 applied, exact p values, and sample sizes (n) are reported in the corresponding figures and
720 figure legends. Data distribution was assessed where appropriate, and statistical tests were
721 selected accordingly. Unless otherwise stated, all statistical tests were two-tailed, and statistical
722 significance was defined as $p < 0.05$.
723
724 **Acknowledgments**
725 We thank the members of the Woolf laboratory for inputs and discussions. We thank the
726 IDDRC Animal Behavior and Physiology Core, funded by NIH/NICHD P50HD105351 and
727 Cellular Imaging Core, funded by NIH P50 HD105351 and Viral Core, funded by NIH
728 5P30EY012196 at Boston Children's Hospital; Dr. Mark L. Andermann for helpful comments
729 and Dr. Fan Wang for general support. This study is supported by the National Institutes of
730 Health grants R01AT011447 and R35NS105076 (C.J.W.), R01DK135707 and R01DK130836
731 (M.R), and the William Randolph Hearst Fund (Y.T.C). Schematics and illustrations were
732 adapted from BioRender.com.
733
734 **Author Contributions**
735 Y.T.C and C.J.W. conceived and designed the study. Y.T.C performed all the experiments and
736 analyzed the data, with assistance from N.M.B. (AAV injections and histology), Y.J. (behavior
737 scoring and RNAscope), J.R.R. (behavior scoring and histology), M.D.S. (GI transit assay and
738 colon histopathology), P.E.M. (barostat recording), Y.L. (fiber photometry), O.B. (automatic
739 behavior screening), K.H. (histology), B.Z. (behavior scoring) and B.L.T. (behavior assays).
740 M.R. provided resources and oversight of the colon histopathology, GI transit and barostat
741 recording experiments. Y.T.C and C.J.W. prepared the figures and wrote the manuscript with
742 inputs from all the authors.

**Disclosures**

C.J.W. is a founder of Nocion Therapeutics, Quralis, and BlackBox Bio, and serves on the scientific advisory boards of Lundbeck Pharma, Axonis, Niroda, Mimetic Medicine, Tenvie Therapeutics, and Tafalgie Therapeutics. M.R. collaborates with Fzata and her spouse is a Novo Nordisk employee.

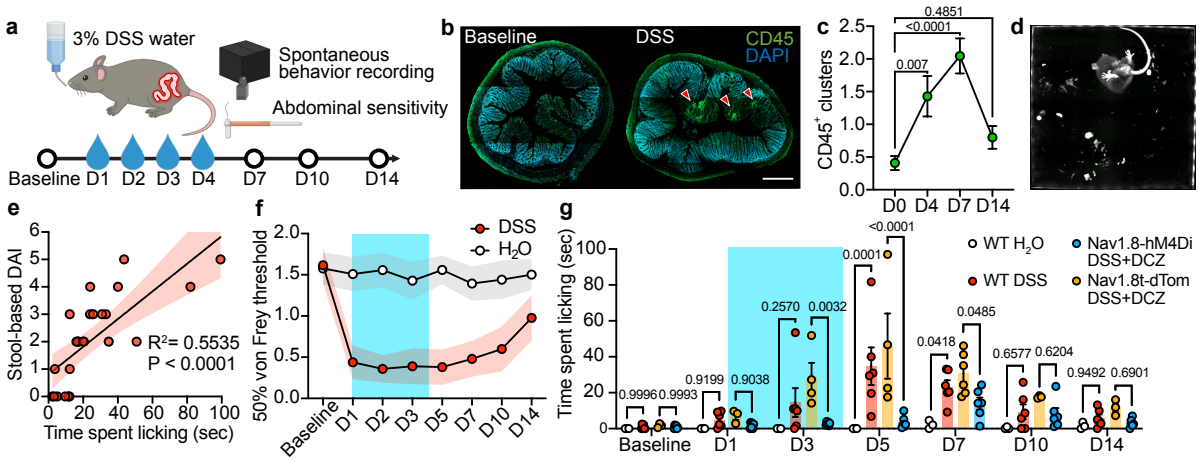


**Fig 1. Nocifensive behaviors elicited in response to DSS-induced colitis.** (a) Schematic of experimental timeline to evaluate spontaneous behavior and abdominal sensitivity in mice treated with 4-day of 3% dextran sodium sulfate (DSS) in their drinking water. (b) Histological verification of immune cell cluster ($CD45^+$, green) invasion into the lamina propria of the mouse colon 3 days post 4-day DSS treatment (right) compared with baseline (left). Scale bar, 20 mm. (c) Quantification of $CD45^+$ clusters at D0 (n=22 from 4 mice), D4 (n=14 from 3 mice), D7 (n=22 from 4 mice) and D14 (n=15 from 3 mice). One-way ANOVA with Dunnett's multiple comparisons. (d) Example of a mouse with DSS-colitis engaged lower body licking behavior. (e) Linear regression analysis between the stool-based disease activity index and time spent licking over a 30-min recording session in mice exposed to DSS (n=25 mice). Light shaded areas represent 95% confidence band. (f) 50% cutaneous mechanical threshold of the mouse lower abdomen using an up-down von Frey test ($H_2O$ n=9 mice, DSS n=9 mice). Light blue shade: 3% DSS drinking water from D1-D4. (g) Automatic licking behavior quantified using a supervised machine learning classifier in WT mice with $H_2O$ (n=3), WT mice with 4-day DSS (n=6), Nav1.8-tdTom mice with 4-day DSS (n=3-6) and Nav1.8-hM4Di mice with 4-day DSS (n=6). In two Nav1.8 groups, the chemogenetic agonist deschloroclozapine (DCZ, 0.1 mg/kg) was injected i.p. at D1, 2, 3 and D4, once per day (two-way ANOVA with Tukey's multiple comparisons).

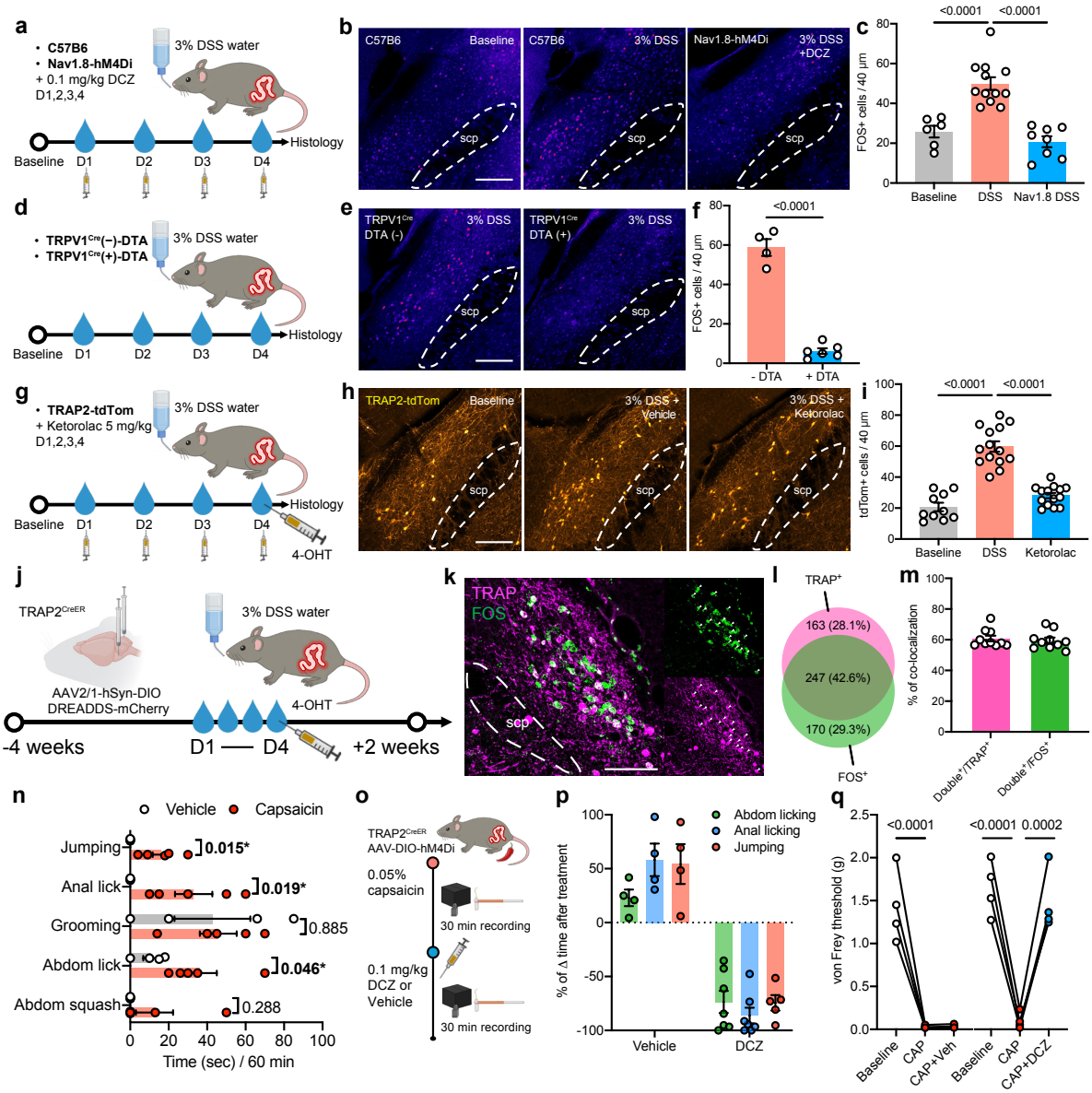


**Fig 2. PBN$^{colitis}$ neurons modulate behavioral responses to nociception in the colon.** (a) Experimental scheme to measure FOS activation in the lateral parabrachial nucleus (PBN$_L$) in WT and Nav1.8-hM4Di mice with 3% DSS drinking water. (b) Histological images of FOS antibody staining in PBN$_L$ region at baseline, with exposure to 3% DSS and after Nav1.8 chemogenetic silencing. scp, superior cerebellar peduncle. Scale bar, 200 µm. (c) Quantification of FOS-positive signals (baseline n=3 mice, DSS n=6 mice, Nav1.8-hM4Di n=4 mice, one-way ANOVA with Tukey's multiple comparisons). (d) Experimental scheme to measure PBN$_L$ FOS activation in TRPV1$^{Cre}$(-)-DTA and TRPV1$^{Cre}$(+)-DTA mice with DSS. (e) Histological images of FOS staining in PBN$_L$ region of TRPV1$^{Cre}$(-)-DTA and TRPV1$^{Cre}$(+)-DTA mice with DSS. Scale bar, 200 µm. (f) Quantification of FOS-positive neurons (TRPV1$^{Cre}$(-) n=2 mice, TRPV1$^{Cre}$(+) n=3 mice, two-tailed unpaired t-test). (g)

Experimental scheme to quantify $PBN_L$ FOS activation using TRAP2-tdTom mice under DSS treatment with i.p. injections of vehicle or 5 mg/kg ketorolac from D1-D4. (h) Histological images of $tdTom^+$ cells in $PBN_L$ region at baseline, 3% DSS with vehicle injections and 3% DSS with ketorolac injections. Scale bar, 200 µm. (i) Quantification of $tdTom^+$ cells (baseline n=5 mice, DSS+vehicle n=7 mice, DSS+ketorolac n=7 mice, one-way ANOVA with Tukey's multiple comparisons). (j) Experimental strategy to functionally label DSS colitis-activated parabrachial neurons ($PBN^{colitis}$) using TRAP2-$Cre^{ER}$ mice injected with Cre-dependent AAV vectors encoding chemogenetic actuators (hM4Di or hM3Dq) bilaterally into $PBN_L$ followed by an i.p. injection of 4-hydroxytamoxifen (4-OHT, 10 mg/kg) to drive expression of FOS-positive cells after 4-day of 3% DSS treatment. (k) Histological verification of signal overlap between TRAPed $PBN^{colitis}$ cells (magenta) and FOS RNAscope (green) under DSS colitis. Scale bar, 200 µm. White arrowheads indicate overlapping signals. (l) Pie chart depicting overlap between $TRAP^+$ and $FOS^+$ neurons. (m) Quantification of signal overlaps in $TRAP^+$ versus $FOS^+$ population (n=5 mice). (n) Quantification of spontaneous pain-related behaviors in response to an intracolonic 0.05% capsaicin infusion over a 60-min recording session (vehicle n=4 mice, capsaicin n=5 mice, multiple unpaired t-tests using two-stage step-up method (Benjamini, Krieger and Yekutieli)). (o) Experimental timeline to evaluate the effect of silencing $PBN^{colitis}$ neurons on capsaicin-induced spontaneous and evoked nocifensive responses. (p) Percentage time difference of capsaicin-induced abdominal licking, peri-anal licking and jumping after vehicle or 0.1 mg/kg DCZ to silence $PBN^{colitis}$ activity in a 30-min recording session (vehicle n=4 mice, DCZ n=5-7 mice). (q) Cutaneous threshold of mouse lower abdomen using up-down von Frey test (vehicle group n=4 mice, DCZ group n=4 mice, one-way ANOVA with Tukey's multiple comparisons).

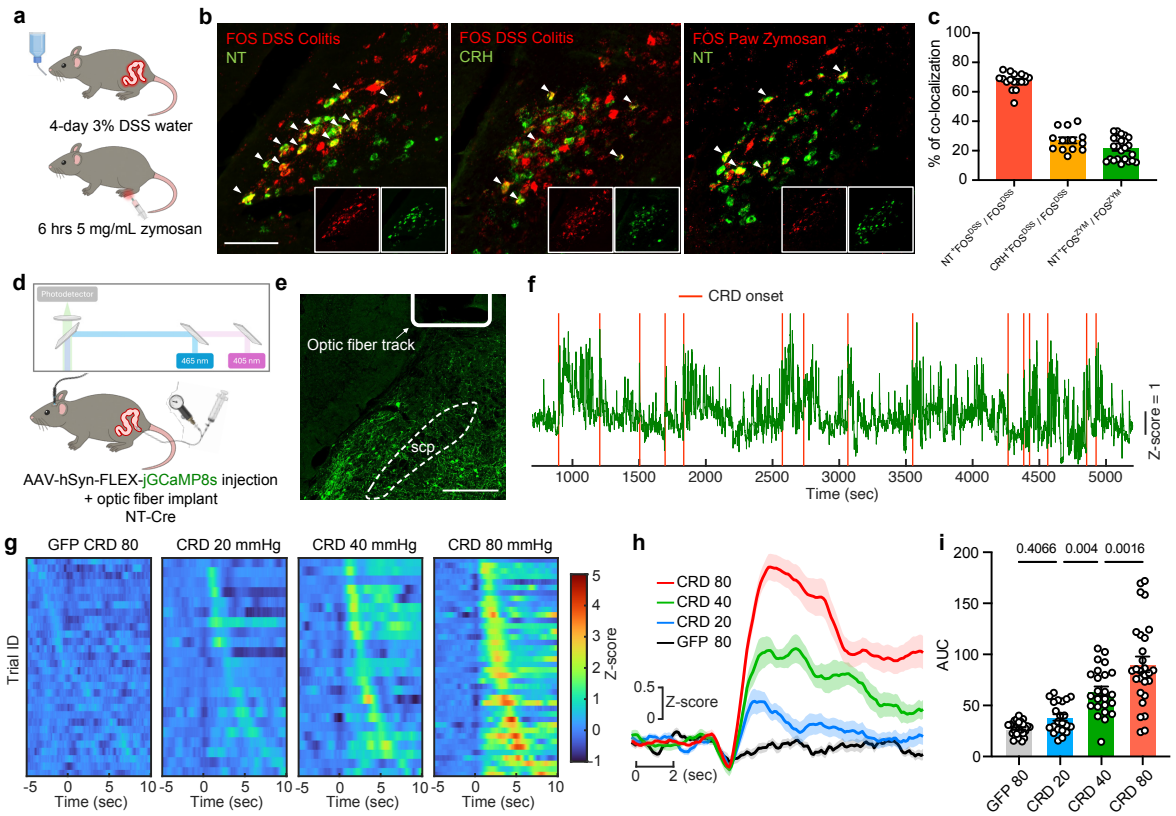


**Fig 3. PBN$_L$ neurotensin neurons encode colon-derived nociceptive signals.** (a) Schematic of colitis-induced visceral pain in mice exposed to 4-day of 3% DSS drinking water (top) and somatosensory inflammatory pain induced by an injection of 5 mg/mL zymosan into plantar surface of the left hindpaw (bottom). (b) PBN$_L$ sections with RNAscope detecting DSS colitis-activated FOS and neurotensin (NT) (left), DSS FOS and corticotropin-releasing hormone (CRH) (middle), and contralateral PBN$_L$ sections with left hindpaw zymosan-activated FOS and NT (right). Scale bar, 200 µm. (c) Quantification of signal overlap between FOS DSS and NT (red bar), FOS DSS and CRH (orange bar), FOS Zymosan and NT marker (green bar). N = 17 sections from 4 mice, 13 sections from 4 mice and 24 sections from 5 mice. (d) Schematic of fiber photometric recordings of neural activity in PBN$_L$ NT neurons evoked by intracolonic balloon distension. (e) Histological verification of AAV-transfected jGCaMP8s cells and fiber implant track in PBN of an NT-Cre mouse. Scale bar, 300 µm. (f) Example z-scored ΔF/F of GCaMP8s signal in NT neurons in response to colorectal distension (CRD) of 80 mmHg. (g) Heatmap responses of PBN$_L$ NT neural activity to 10-sec CRD at 20, 40, 80 mmHg and GFP controls in response to CRD at 80 mmHg (GFP n=30 trials from 3 mice, CRD 20 n=22, CRD 40 n=24, CRD 80 n=40 trials from 5 mice). (h) CRD-triggered average z-scored ΔF/F of NT neurons. Light shaded areas represent s.e.m. (i) Area under curve (AUC) measured using

average signal during the 5 sec prior to CRD onset as baseline, from (h). One-way ANOVA with Tukey's multiple comparisons.

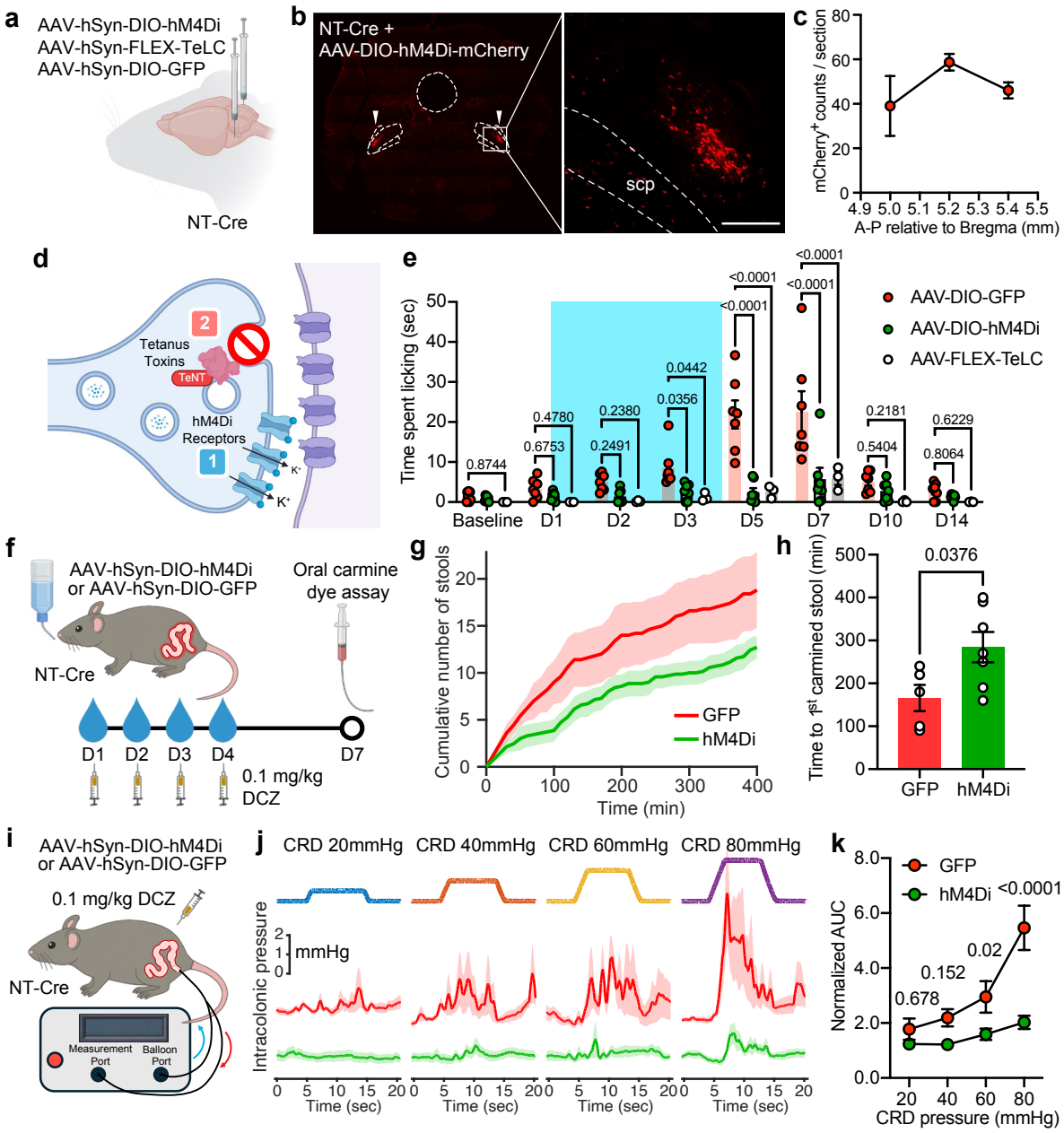


**Fig 4. PBN$_L$ neurotensin neurons control behavior and visceral sensitivity induced by colonic insults.** (a) Schematic of two different silencing (hM4Di: modified human M4 muscarinic receptor for chemogenetic silencing, TeLC: tetanus toxin light chain-mediated synaptic impairment) and a control AAV GFP injection to measure causal function of PBN$_L$ NT neurons. (b) Histological verification of Cre-dependent AAV injections into bilateral PBN$_L$ of an NT-Cre mouse, scp, superior cerebellar peduncle. Scale bar, 200 µm. (c) Quantification of mCherry$^+$ cells in the PBN$_L$ at A-P axis 5.0, 5.2 and 5.4 mm relative to bregma (n=3 mice). (d) Diagram illustrating two different silencing strategies (1) virally mediated Gi-coupled muscarinic receptors induce an efflux of potassium ions for temporary neural hyperpolarization (2) virally mediated tetanus toxin light chain blocks a presynaptic fusion protein for long-term

abrogation of neurotransmitter release. (e) Licking behavior quantified using a supervised machine-learning classifier in NT-Cre mice with bilateral injections of a Cre-dependent AAV that encodes GFP (n=7 mice), or hM4Di (n=7 mice) and TeLC (n=3 mice) in mice subjected to 4-day 3% DSS treatment. In both the GFP and hM4Di groups, the chemogenetic agonist (DCZ; 0.1 mg $kg^{-1}$, i.p.) was injected once daily on D1-D4. Two-way ANOVA with Dunnett's multiple comparisons. (f) Experimental scheme to evaluate gastrointestinal transit using a carmine-red dye assay to measure latency of the first appearance of dye-colored stool following oral administration on D7. GFP and hM4Di mice underwent 4-day DSS treatment and received DCZ injection once per day from D1-D4. (g) Quantification of total stool number 30 min after an oral gavage of carmine dye followed by stool count every 10-min until 400 min (GFP n=5 mice, hM4Di n=7 mice). Light shaded areas represent s.e.m. (h) Quantification of latency to first carmine-dyed stool (GFP n=5 mice, hM4Di n=7 mice. Two-tailed unpaired t-test). (i) Schematic of colonic reflex response to graded distensions by an inserted balloon connected to a close-loop, calibrated barostat system. (j) CRD-triggered average intracolonic pressure responses to distension pressures of 20, 40, 60 and 80 mmHg in GFP (red, n=8 trials from 4 mice) or hM4Di (green, n=14 trials from 7 mice) mice. Light shaded areas represent s.e.m. (k) Quantification of normalized AUC (average of 5-sec AUC following CRD onset / average of 5-sec AUC prior to CRD onset) in response to CRD pressure at 20, 40, 60 and 80 mmHg in GFP (red, n=4 mice) and hM4Di (green, n=7 mice) group. Two-way ANOVA with Šídák's multiple comparisons.

## References


1 Bielefeldt, K., Davis, B. & Binion, D. G. Pain and inflammatory bowel disease. *Inflamm Bowel Dis* **15**, 778–788 (2009). https://doi.org/10.1002/ibd.20848

2 Coates, M. D. *et al.* Abdominal Pain in Inflammatory Bowel Disease: An Evidence-Based, Multidisciplinary Review. *Crohns Colitis 360* **5**, otad055 (2023). https://doi.org/10.1093/crocol/otad055

3 Yang, D. *et al.* Nociceptor neurons direct goblet cells via a CGRP-RAMP1 axis to drive mucus production and gut barrier protection. *Cell* **185**, 4190–4205 e4125 (2022). https://doi.org/10.1016/j.cell.2022.09.024

4 Drewes, A. M. *et al.* Gastrointestinal pain. *Nat Rev Dis Primers* **6**, 1 (2020). https://doi.org/10.1038/s41572-019-0135-7

5 Rao, M. An increasingly complex view of intestinal motility. *Nat Rev Gastroenterol Hepatol* **17**, 72–73 (2020). https://doi.org/10.1038/s41575-019-0249-0

6 Defaye, M., Nasser, Y. & Altier, C. Mechanisms of chronic abdominal pain in inflammatory bowel disease and implications for treatment. *Nat Rev Gastroenterol Hepatol* (2025). https://doi.org/10.1038/s41575-025-01139-8

7 Takahashi, K. *et al.* Post-inflammatory Abdominal Pain in Patients with Inflammatory Bowel Disease During Remission: A Comprehensive Review. *Crohns Colitis 360* **3**, otab073 (2021). https://doi.org/10.1093/crocol/otab073

8 Latremoliere, A. & Woolf, C. J. Central sensitization: a generator of pain hypersensitivity by central neural plasticity. *J Pain* **10**, 895–926 (2009). https://doi.org/10.1016/j.jpain.2009.06.012

9 Woolf, C. J. Central sensitization: implications for the diagnosis and treatment of pain. *Pain* **152**, S2–S15 (2011). https://doi.org/10.1016/j.pain.2010.09.030

10 Zeng, X., Powell, R. & Woolf, C. J. Mechanism-based nonopioid analgesic targets. *J Clin Invest* **135** (2025). https://doi.org/10.1172/JCI191346

11 Alexandre, C. *et al.* Nociceptor spontaneous activity is responsible for fragmenting non-rapid eye movement sleep in mouse models of neuropathic pain. *Sci Transl Med* **16**, eadg3036 (2024). https://doi.org/10.1126/scitranslmed.adg3036

12 Chiang, M. C. *et al.* Divergent Neural Pathways Emanating from the Lateral Parabrachial Nucleus Mediate Distinct Components of the Pain Response. *Neuron* **106**, 927–939 e925 (2020). https://doi.org/10.1016/j.neuron.2020.03.014

13 Han, S., Soleiman, M. T., Soden, M. E., Zweifel, L. S. & Palmiter, R. D. Elucidating an Affective Pain Circuit that Creates a Threat Memory. *Cell* **162**, 363–374 (2015). https://doi.org/10.1016/j.cell.2015.05.057

14 Palmiter, R. D. The Parabrachial Nucleus: CGRP Neurons Function as a General Alarm. *Trends Neurosci* **41**, 280–293 (2018). https://doi.org/10.1016/j.tins.2018.03.007

15 Rodriguez, E. *et al.* A craniofacial-specific monosynaptic circuit enables heightened affective pain. *Nat Neurosci* **20**, 1734–1743 (2017). https://doi.org/10.1038/s41593-017-0012-1

16 Choi, S. *et al.* Parallel ascending spinal pathways for affective touch and pain. *Nature* **587**, 258–263 (2020). https://doi.org/10.1038/s41586-020-2860-1

17 Yarmolinsky, D. A. *et al.* Differential modification of ascending spinal outputs in acute and chronic pain states. *Neuron* **113**, 1223–1239 e1225 (2025). https://doi.org/10.1016/j.neuron.2025.01.031

18 Huang, T. *et al.* Identifying the pathways required for coping behaviours associated with sustained pain. *Nature* **565**, 86–90 (2019). https://doi.org/10.1038/s41586-018-0793-8

19 Goldstein, N. *et al.* A parabrachial hub for need-state control of enduring pain. *Nature* **647**, 689–697 (2025). https://doi.org/10.1038/s41586-025-09602-x
20 Nardone, S. *et al.* A spatially-resolved transcriptional atlas of the murine dorsal pons at single-cell resolution. *Nat Commun* **15**, 1966 (2024). https://doi.org/10.1038/s41467-024-45907-7
21 Pauli, J. L. *et al.* Molecular and anatomical characterization of parabrachial neurons and their axonal projections. *Elife* **11** (2022). https://doi.org/10.7554/eLife.81868
22 Yao, Z. *et al.* A high-resolution transcriptomic and spatial atlas of cell types in the whole mouse brain. *Nature* **624**, 317–332 (2023). https://doi.org/10.1038/s41586-023-06812-z
23 Ma, Q. A functional subdivision within the somatosensory system and its implications for pain research. *Neuron* **110**, 749–769 (2022). https://doi.org/10.1016/j.neuron.2021.12.015
24 Chiang, M. C. *et al.* Parabrachial Complex: A Hub for Pain and Aversion. *J Neurosci* **39**, 8225–8230 (2019). https://doi.org/10.1523/JNEUROSCI.1162-19.2019
25 Li, Y. *et al.* Tachykinin signaling in the right parabrachial nucleus mediates early-phase neuropathic pain development. *Neuron* **113**, 605–619 e606 (2025). https://doi.org/10.1016/j.neuron.2024.11.021
26 Condon, L. F. *et al.* Parabrachial Calca neurons drive nociplasticity. *Cell Rep* **43**, 114057 (2024). https://doi.org/10.1016/j.celrep.2024.114057
27 Chassaing, B., Aitken, J. D., Malleshappa, M. & Vijay-Kumar, M. Dextran sulfate sodium (DSS)-induced colitis in mice. *Curr Protoc Immunol* **104**, 15 25 11–15 25 14 (2014). https://doi.org/10.1002/0471142735.im1525s104
28 Wirtz, S. *et al.* Chemically induced mouse models of acute and chronic intestinal inflammation. *Nat Protoc* **12**, 1295–1309 (2017). https://doi.org/10.1038/nprot.2017.044
29 Barkai, O. *et al.* A machine learning tool with light-based image analysis for automatic classification of 3D pain behaviors. *Cell Rep Methods* **5**, 101145 (2025). https://doi.org/10.1016/j.crmeth.2025.101145
30 Zhang, Z. *et al.* Automated preclinical detection of mechanical pain hypersensitivity and analgesia. *Pain* **163**, 2326–2336 (2022). https://doi.org/10.1097/j.pain.0000000000002680
31 Nagai, Y. *et al.* Deschloroclozapine, a potent and selective chemogenetic actuator enables rapid neuronal and behavioral modulations in mice and monkeys. *Nat Neurosci* **23**, 1157–1167 (2020). https://doi.org/10.1038/s41593-020-0661-3
32 Liu, S. *et al.* Divergent brainstem opioidergic pathways that coordinate breathing with pain and emotions. *Neuron* **110**, 857–873 e859 (2022). https://doi.org/10.1016/j.neuron.2021.11.029
33 Jain, A. *et al.* Nociceptor-immune interactomes reveal insult-specific immune signatures of pain. *Nat Immunol* **25**, 1296–1305 (2024). https://doi.org/10.1038/s41590-024-01857-2
34 Sammons, M. *et al.* Brain-body physiology: Local, reflex, and central communication. *Cell* **187**, 5877–5890 (2024). https://doi.org/10.1016/j.cell.2024.08.050
35 Meerschaert, K. A. & Chiu, I. M. The gut-brain axis and pain signalling mechanisms in the gastrointestinal tract. *Nat Rev Gastroenterol Hepatol* **22**, 206–221 (2025). https://doi.org/10.1038/s41575-024-01017-9

36 Wang, H. *et al.* A tool kit of highly selective and sensitive genetically encoded neuropeptide sensors. *Science* **382**, eabq8173 (2023). https://doi.org/10.1126/science.abq8173

37 Gebhart, G. F. & Bielefeldt, K. Physiology of Visceral Pain. *Compr Physiol* **6**, 1609–1633 (2016). https://doi.org/10.1002/cphy.c150049

38 Campos, C. A., Bowen, A. J., Roman, C. W. & Palmiter, R. D. Encoding of danger by parabrachial CGRP neurons. *Nature* **555**, 617–622 (2018). https://doi.org/10.1038/nature25511

39 Van Oudenhove, L. *et al.* Common and distinct neural representations of aversive somatic and visceral stimulation in healthy individuals. *Nat Commun* **11**, 5939 (2020). https://doi.org/10.1038/s41467-020-19688-8

40 Wolfson, R. L. *et al.* DRG afferents that mediate physiologic and pathologic mechanosensation from the distal colon. *Cell* **186**, 3368–3385 e3318 (2023). https://doi.org/10.1016/j.cell.2023.07.007

41 Gao, X. *et al.* Calcium imaging in population of dorsal root ganglion neurons unravels novel mechanisms of visceral pain sensitization and referred somatic hypersensitivity. *Pain* **162**, 1068–1081 (2021). https://doi.org/10.1097/j.pain.0000000000002096

42 Gazit Shimoni, N. *et al.* Changes in neurotensin signalling drive hedonic devaluation in obesity. *Nature* **641**, 1238–1247 (2025). https://doi.org/10.1038/s41586-025-08748-y

43 Li, H. *et al.* Neurotensin orchestrates valence assignment in the amygdala. *Nature* **608**, 586–592 (2022). https://doi.org/10.1038/s41586-022-04964-y

44 Guo, R. *et al.* Arrestin-biased allosteric modulator of neurotensin receptor 1 alleviates acute and chronic pain. *Cell* **188**, 4332–4349 e4321 (2025). https://doi.org/10.1016/j.cell.2025.04.038

45 Castagliuolo, I. *et al.* Neurotensin is a proinflammatory neuropeptide in colonic inflammation. *J Clin Invest* **103**, 843–849 (1999). https://doi.org/10.1172/JCI4217

46 Gui, X., Liu, S., Yan, Y. & Gao, Z. Neurotensin receptor 1 overexpression in inflammatory bowel diseases and colitis-associated neoplasia. *World J Gastroenterol* **19**, 4504–4510 (2013). https://doi.org/10.3748/wjg.v19.i28.4504

47 Law, I. K. *et al.* Neurotensin--regulated miR-133alpha is involved in proinflammatory signalling in human colonic epithelial cells and in experimental colitis. *Gut* **64**, 1095–1104 (2015). https://doi.org/10.1136/gutjnl-2014-307329

48 Udit, S., Blake, K. & Chiu, I. M. Somatosensory and autonomic neuronal regulation of the immune response. *Nat Rev Neurosci* **23**, 157–171 (2022). https://doi.org/10.1038/s41583-021-00555-4

49 Mathis, A. *et al.* DeepLabCut: markerless pose estimation of user-defined body parts with deep learning. *Nat Neurosci* **21**, 1281–1289 (2018). https://doi.org/10.1038/s41593-018-0209-y

50 Gonzalez-Cano, R. *et al.* Up-Down Reader: An Open Source Program for Efficiently Processing 50% von Frey Thresholds. *Front Pharmacol* **9**, 433 (2018). https://doi.org/10.3389/fphar.2018.00433

51 Christianson, J. A. & Gebhart, G. F. Assessment of colon sensitivity by luminal distension in mice. *Nat Protoc* **2**, 2624–2631 (2007). https://doi.org/10.1038/nprot.2007.392

52 Muppirala, A. N. *et al.* Tachykinin signaling defines distinct populations of glia in the enteric nervous system. *Neuron* (2026). https://doi.org/10.1016/j.neuron.2025.11.030